NANO LETTERS

Letter

pubs.acs.org/NanoLett

Gate-Tunable Large Negative Tunnel Magnetoresistance in Ni−C_{60}−Ni Single Molecule Transistors

Kenji Yoshida,*[,†] Ikutaro Hamada,[‡,§] Shuichi Sakata,[†] Akinori Umeno,[†] Masaru Tsukada,[‡,§] and Kazuhiko Hirakawa*[,†,§]

[†]Institute of Industrial Science and Institute for Nano Quantum Information Electronics, University of Tokyo, 4-6-1 Komaba, Meguro-ku, Tokyo 153-8505, Japan

[‡]Advanced Institute for Materials Research (AIMR), Tohoku University, Sendai 980-8577, Japan

[§]CREST-Japan Science and Technology Agency, Kawaguchi, Saitama 332-0012, Japan

S *Supporting Information*

ABSTRACT: We have fabricated single C_{60} molecule transistors with ferromagnetic Ni leads (FM-SMTs) by using an electrical break junction method and investigated their magnetotransport. The FM-SMTs exhibited clear gate-dependent hysteretic tunnel magnetoresistance (TMR) and the TMR values reached as high as −80%. The polarity of the TMR was found to be always negative over the entire bias range studied here. Density functional theory calculations show that hybridization between the Ni substrate states and the C_{60} molecular orbitals generates an antiferromagnetic configuration in the local density of states near the Fermi level, which gives a reasonable explanation for the observed negative TMR.

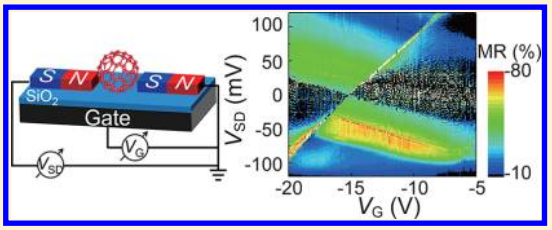

KEYWORDS: *Molecular electronics, spintronics, tunnel magnetoresistance, nanogap electrodes, single electron transistors*

Spin-dependent transport through organic molecules is a key to molecular spintronics. Recent progress in nanofabrication technologies has made it possible to fabricate nanometer-scale gaps in metal electrodes that can be used to electrically contact single molecules.[1−5] A number of intriguing quantum transport phenomena characteristic of single molecule junctions have been reported so far.[5−9] For spintronic device applications, organic molecules are suitable because they are mainly composed of light elements, which have weak spin−orbit interactions and consequently long spin-relaxation times. Therefore, it is of prime importance to understand electronic structures of single molecule junctions with ferromagnetic electrodes (FM-SMJs) and spin-dependent transport in such structures.[10,11]

A number of interesting spin-related phenomena such as Kondo effect,[12] large anisotropic magnetoresistance (AMR),[13] and giant magnetoresistance (GMR)[14] have been reported in previous studies on FM-SMJs. However, these works presented only two-terminal current−voltage (I−V) data. Since changes in magnetization of FM electrodes in single electron tunneling devices are accompanied by various effects that give rise to resistance changes,[15−20] two-terminal I−V data only are not sufficient to elucidate the origins of resistance changes; systematic investigation on electron transport in single molecule transistors (SMTs) with gate electrodes is necessary.

In this study, we have investigated tunnel magnetoresistance (TMR) in single C_{60} molecule transistors with ferromagnetic Ni leads (FM-SMTs). By applying the feedback-controlled electrical break junction (FC-EBJ) method[21] to Ni nanojunctions,[22−24] we have successfully fabricated FM-SMTs. We demonstrate that TMR of FM-SMTs can be controlled by gate-electric fields and TMR values reach as high as −80%. The polarity of the TMR was always negative over the entire bias range studied here. We have calculated the local electronic structure for the C_{60}/Ni(111) interface in the framework of density functional theory and showed that hybridization between the Ni 3d states and the C_{60} molecular orbitals modulates the spin-polarization of the local density of states near the Fermi level and generates an antiferromagnetic configuration there. This physical picture qualitatively explained the observed negative TMR.

The 15 nm thick Ni nanojunctions used in this work were fabricated on a 100 nm thick surface oxide layer grown on heavily p-type doped Si substrates by using electron-beam lithography and electron-beam evaporation. As shown in Figure 1b, we employed an asymmetrical shape design for the Ni nanojunctions; they are expected to undergo magnetic reversal at different magnetic fields due to shape anisotropy. We then deposited a few drops of a dilute toluene solution of C_{60} onto the Ni nanojunctions and immediately dried off the solution by nitrogen gas blow. After depositing the molecules, we mounted the samples into a ^{3}He cryostat and applied the FC-EBJ method to the Ni nanojunctions to create nanometer-scale gaps. Details of the feedback control scheme in the electrical

Received: October 20, 2012
Revised: January 16, 2013

   dx.doi.org/10.1021/nl303871x | *Nano Lett.* XXXX, XXX, XXX−XXX

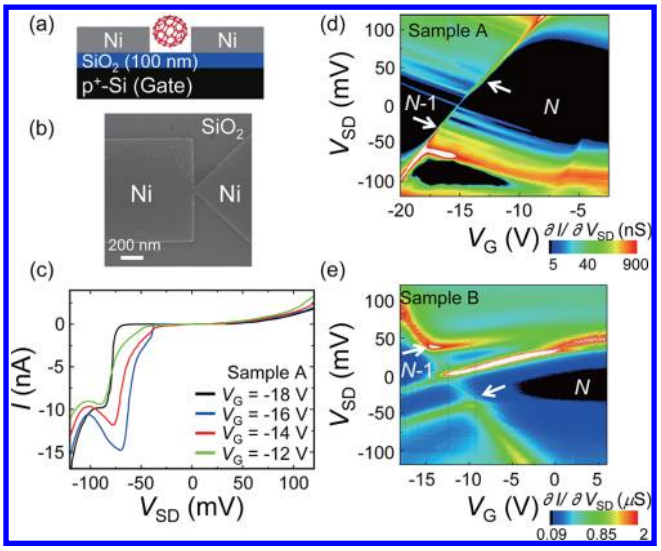

Figure 1. (a) A schematic diagram of a single C_{60} molecule transistor. (b) A scanning electron microscope image of a fabricated Ni nanojunction before the electrical break junction process. (c) Current−voltage (I−V_{SD}) curves taken at V_G at 300 mK for a C_{60} transistor with Ni electrodes (sample A). (d,e) Coulomb stability diagrams for sample A and sample B, respectively. $\partial I/\partial V_{SD}$ is plotted by a logarithmic color scale and 5 nS (90 nS) and 900 nS (2 μS) for sample A (sample B) correspond to blue and red, respectively. $\partial I/\partial V_{SD}$ lower than 5 nS (90 nS) and higher than 900 nS (2 μS) for sample A (sample B) are expressed as black and white, respectively. A black-colored area appearing in the transport regime where $V_{SD} < 0$ in (d) corresponds to negative differential conductance. White arrows indicate the excited energy states that correspond to an internal vibrational mode (the $H_g(1)$ mode) of C_{60} molecules. N in (d,e) denotes the electron number in the C_{60} molecules.

break junction method used in this work were described elsewhere.[25] We carried out transport measurements on the fabricated samples in vacuum at 0.3 K. The p-type Si substrate was used as a back gate. We measured 186 junctions and five samples clearly exhibited gate-dependent I−V characteristics and were stable enough for detailed measurements.

Typical I−V characteristics measured on a sample at various gate voltages, V_G, are shown in Figure 1c. As clearly seen in the figure, the current is suppressed at low source−drain bias voltages, V_{SD}, and increases in a stepwise manner with increasing V_{SD}. The size of the conductance-suppressed region is modulated by the gate voltage, V_G. These features are characteristic of single electron tunneling. Figure 1d,e shows differential conductance ($\partial I/\partial V_{SD}$) spectra calculated by numerical differentiation as a function of V_{SD} and V_G obtained for two samples (sample A and B). As seen in the figures, there are crossing lines that separate the high-conductance single electron tunneling regions from the conductance-suppressed Coulomb blockaded regions. In the Coulomb stability diagrams of both samples, excitations are commonly observed at around 35 meV, as denoted by white arrows in Figure 1d,e. The observed excitation energy is consistent with that of an internal vibrational mode of C_{60} molecules (the $H_g(1)$ mode),[6,26] indicating that the Coulomb islands in the samples are single C_{60} molecules and that SMTs with FM electrodes are successfully fabricated. The crossing points (charge degeneracy points) for our five Ni−C_{60} SMTs studied here were always located in the range of -17 V $< V_G < -11$ V, suggesting that clean Ni/C_{60} interfaces are reproducibly obtained. From these Coulomb stability diagrams, the addition energy, E_A, for the Coulomb diamonds around $V_G = V_{SD} = 0$ was estimated to be more than 120 meV, which is comparable to E_A previously reported for C_{60}-based SMTs.[27,28] Our experiments did not allow us to precisely determine the number of electrons, N, in the C_{60} molecules in the fabricated devices. However, our DFT calculations (see below) and the Bader charge analysis[29] predict that when C_{60} molecules are placed on the Ni(111) surface, 0.9 electrons are transferred from the Ni metal to the C_{60} molecules. Moreover, it has been reported that when the C_{60} molecules are placed on the more reactive Ni (110) surface, 2 ± 1 electrons are transferred from the Ni surface to the C_{60} molecules.[30] Therefore it is reasonable to assume that N is in the range from 1 to 2 when $V_G = V_{SD} = 0$ (see Figure 1d,e). Furthermore, it is found that the slopes of the two boundaries of the Coulomb diamonds are different. This indicates that the captured C_{60} molecules are closer to one of the electrodes and couple more strongly with it. It should be noted in Figure 1c,d that a negative differential conductance (NDC) appeared in the negative V_{SD} region for Sample A. We found that the NDC was gradually suppressed as magnetic fields were increased from 1 to 8 T (not shown here). Although the origin of the NDC is not clear, the observed magnetic field dependence suggests that the NDC may be due to tunneling via spin-related states at Ni/C_{60} interfaces.

Figure 2 shows MR curves measured on sample A at V_{SD} = 20 mV at three different V_G's (−14, −16, and −18 V) for

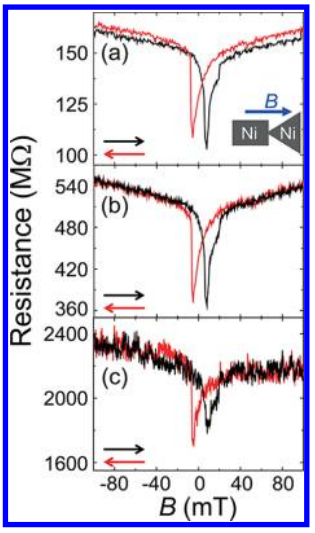

Figure 2. (a−c) Magnetoresistances of sample A measured at 0.3 K for V_G = −14, −16, and −18 V, respectively. V_{SD} was set to be 20 mV. The inset in (a) shows a schematic geometry of a pair of Ni electrodes and an applied B-field (in-plane and parallel to the current). The black (red) arrow indicates the positive (negative) B-field sweep.

sweep-up and -down of an external magnetic field, B. B was applied in-plane and parallel to the current. As clearly seen in Figure 2, negative hysteretic changes in the sample resistance were observed between −1.2 and 25.2 mT (−13 and 20 mT) in the positive (negative) sweep direction, indicating that the magnetization configuration of the two Ni electrodes switches from the parallel (P) to the antiparallel (AP) state at these fields. The minimum of the sample resistance is found for an 8 mT (−6 mT) B-field for the positive (negative) sweep direction and does not depend on V_G. Here, we define the TMR as (R_{AP} − R_P)/R_{AP}, where R_{AP} and R_P are the AP- and P-state

dx.doi.org/10.1021/nl303871x | Nano Lett. XXXX, XXX, XXX−XXX

resistances, respectively. The TMR was −56.2, −47.2, and −20.8% (−48.3, −45.5, and −28.7%) for the negative (positive) sweep direction at V_G = −14, −16, and −18 V, respectively, indicating that the TMR of FM-SMTs can be controlled by gate electric fields.

Figure 3a shows a color-coded spectrum of the TMR for the sample A as a function of V_{SD} and V_G. As seen in the figure, the

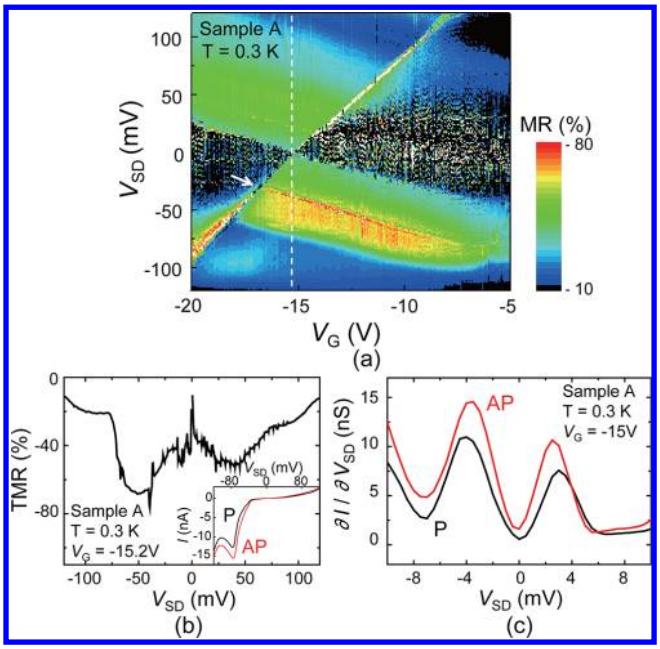

Figure 3. (a) A color-coded spectrum of the TMR as a function of V_{SD} and V_G obtained for sample A at 0.3 K. The TMR value is represented by a color scale from blue (−10%) to red (−80%). (b) TMR is plotted as a function of V_{SD} at V_G = −15.2 V (along the white dotted line in (a)). The inset shows I–V_{SD} curves for parallel (B = −100 mT; black) and antiparallel (B = 8 mT; red) configuration of the magnetization of the Ni electrodes. (c) $\partial I/\partial V_{SD}$ curves as a function of V_{SD} at V_G = −15 V taken at parallel (B = −100 mT; black) and antiparallel (B = 8 mT; red) magnetization configuration of the Ni electrodes.

TMR can be modulated both by V_G and V_{SD} and can be as high as −80% for a certain V_G–V_{SD} condition. It is also found that the sign of the TMR is negative throughout the wide bias condition studied here. In Julliere's model,[31] in which the TMR is determined simply by the spin polarization in the density of states of the two FM electrodes, P_1 and P_2, it is given by TMR $\equiv (R_{AP} - R_P)/R_{AP} = 2P_1P_2/(1 + P_1P_2)$. In this model, the expected value of the TMR for Ni tunnel junctions is +17.5% (P for Ni ∼ 0.31[31]). However, the observed TMR is not only much larger than that expected from Julliere's model, but also has an opposite sign. In addition, while conventional magnetic tunnel junctions show a monotonic decrease in TMR as bias voltages increase,[32] the TMR for the sample did not show such a V_{SD}-dependence (Figure 3b).

As a reference experiment, we fabricated FM tunnel junctions without C_{60} molecules by using the FC-EBJ method. The observed TMRs for the reference FM tunnel junctions varied from sample to sample[22,33] and were typically only a few percent (∼10% at most), that is to say much smaller than those observed for the FM-SMTs (see Supporting Information). Furthermore, the TMRs for bare Ni tunnel junctions decreased monotonically as V_{SD} was increased, which is very different from what was observed for the FM-SMTs. The TMR characteristics observed for the FM-SMTs thus clearly indicate that the C_{60} molecules trapped in the Ni nanogap electrodes play a crucial role in the magnetotransport of the samples.

Before discussing what kind of roles the C_{60} molecules play in the magnetotransport in these FM-SMTs, we need to examine the effect of the electrochemical potential shift in the C_{60} molecule due to a magnetization configuration change of the Ni electrodes upon the observed TMR. In SETs that have FM electrodes, changes in the magnetization configurations of the FM electrodes induce the above-mentioned electrochemical potential shift in the Coulomb island via Zeeman effect, which in turn gives rise to hysteretic resistance changes similar to the conventional MR curve and mimics the spin-valve effect. It is therefore necessary to estimate the magnitude of the electrochemical potential shifts in the present sample. Figure 3c shows $\partial I/\partial V_{SD}$ traces taken at the P and AP configurations for V_G = −15 V. Each peak in the $\partial I/\partial V_{SD}$ traces corresponds to a transition between two successive ground states, GS(N − 1) ↔ GS(N). Although the peak positions for the AP state shift to the lower bias side with respect to those for the P state, the shifts are very small. This means that a shift in electrochemical potential in the C_{60} molecule caused by changes in magnetization configuration is small,[34] suggesting that the factor governing the large negative TMR is spin-dependent electron tunneling through the C_{60} molecule.

Now we discuss the role played by the C_{60} molecule in the magnetotransport in Ni-SMTs. As shown in the previous report on FM/organic molecule/FM junctions,[35,36] hybridization between molecular orbitals and the FM d-orbitals at the metal/molecule interfaces modulates the spin polarization in the local density of states (LDOS) and electron transport becomes strongly spin-dependent. Moreover, reflecting the spin polarization in the LDOS with complex energy dependence, FM molecular junctions may show unique bias-dependent TMR. Therefore, a more detailed understanding of the microscopic electronic structures at the Ni/C_{60} interface is needed to clarify the origin of the observed TMR.

For this purpose, we carried out density functional theory calculation for the C_{60}/Ni(111) interface (see Figure 4a,b), taking into account the van der Waals interaction. Although the precise geometry at the Ni/C_{60} interface of the sample is not known, we believe that the local electronic structure gives us a good qualitative picture of the transport property of Ni-SMTs. All the calculations were carried out using a plane wave basis set and ultrasoft pseudopotentials[37] within the generalized gradient approximation as implemented in the STATE code.[38] The Perdew–Burke–Ernzerhof[39] functional was used for the exchange correlation energy and potential. The van der Waals interaction was introduced by a semiempirical method by Grimme (DFT-D2).[40] The van der Waals density functional (vdW-DF2)[41] accompanied with the C09[42] exchange was also used,[43] and the results with vdW-DF2 were similar to those with DFT-D. A C_{60} molecule was put on one side of the Ni slab, which was modeled by a four-layer slab with a (4 × 4) periodicity, and spurious electrostatic interaction between neighboring slabs[44] was eliminated by using the effective screening medium method.[45] A 2 × 2 k-point set was used for the Brillouin zone integration and a denser 4 × 4 k-point set was used for calculating the DOSs. Figure 4c shows the spin resolved density of states projected onto the molecular orbitals of C_{60} on the Ni(111) surface.

As seen in Figure 4c, spin-dependent hybridization between the Ni 3d states and the lowest unoccupied molecular orbitals

dx.doi.org/10.1021/nl303871x | Nano Lett. XXXX, XXX, XXX–XXX

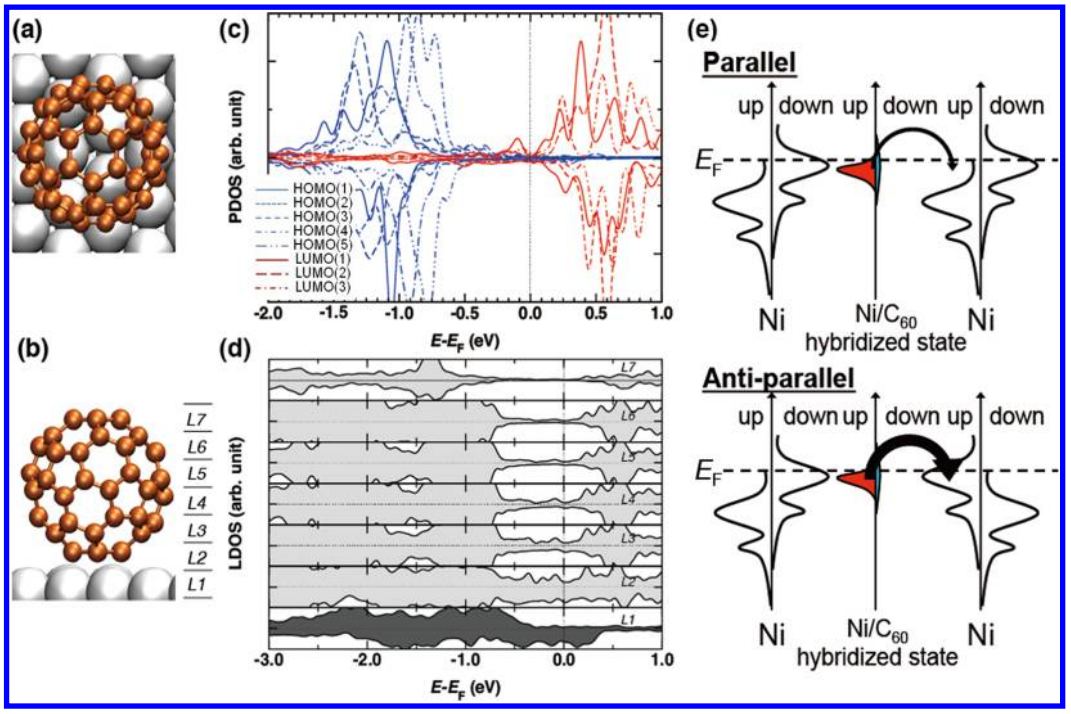

Figure 4. (a) A top view and (b) a side view of a C_{60} molecule on the Ni(111) surface in the most stable configuration. (c) Spin-resolved density of states projected onto the molecular orbitals of C_{60}. (d) Spin-dependent layer-resolved LDOS of the C_{60}/Ni(111) interface. The layer positions are indicated in (b). (e) Schematic representation of spin-resolved density of states and spin-dependent electron tunneling in a Ni/C_{60}/Ni junction when the two Ni electrodes are in the parallel magnetization configuration (upper) and the antiparallel magnetization configuration (lower). The substrate states for the left Ni electrode, which is closer to a C_{60} molecule, hybridize with the C_{60} molecular orbitals.

(LUMOs) of a C_{60} molecule produces spin-polarized molecular states at around −0.1 eV relative to the Fermi level (E_F). The spin-polarization has an energy-dependence, which supports the V_{SD}-dependence of the TMR observed in the present sample. Furthermore, the spin-polarization of the hybridized molecular states at the C_{60}/Ni (111) interface near E_F is found to be reversed with respect to that of the Ni substrate states (see the layer resolved density of states in Figure 4d). As mentioned before, the trapped C_{60} molecule is closer to one of the nanogap Ni electrodes. Assuming that the hybridization occurs only between a C_{60} molecule and the Ni electrode closer to it and that the other Ni electrode serves as a reservoir with spin-dependent DOS, the electron tunneling process in the Ni−C_{60}-Ni junctions can be described as schematically shown in Figure 4e. In the configuration where the two Ni electrodes have a parallel magnetization, spin polarization in the hybridized states in the vicinity of E_F (spin up) is opposite to that of the right Ni electrode (spin down). On the contrary, when the two Ni electrodes are in the antiparallel configuration, the spin polarization near E_F in the hybridized states is aligned with that in the right Ni electrode. Consequently, the antiparallel configuration becomes more conductive than the parallel configuration, which results in the negative TMR and can explain the experimental results.

In summary, we have investigated TMR in single C_{60} molecule transistors with ferromagnetic Ni leads (FM-SMTs). By applying the feedback-controlled electrical break junction method to Ni nanojunctions, we have successfully fabricated FM-SMTs. We demonstrate gate-tunable TMR, which reach as high as −80%. The fabricated devices exhibited the negative TMR over the entire bias range studied here. Spin density functional theory calculations have revealed that hybridization between the Ni substrate states and the C_{60} molecular orbitals modulates the spin-polarization of LDOS and generates antiferromagnetic configuration in the LDOS near the Fermi level. Tunneling through this new hybridized state at the Ni/C_{60} interface is responsible for the observed negative TMR.

■ ASSOCIATED CONTENT

Ⓢ Supporting Information

Supporting Information contains magnetotransport characteristics of bare Ni tunnel junctions fabricated by using the electrical break junction method. This material is available free of charge via the Internet at http://pubs.acs.org.

■ AUTHOR INFORMATION

Corresponding Author

*E-mail: (K.Y.) kyoshida@iis.u-tokyo.ac.jp; (K.H.) hirakawa@iis.u-tokyo.ac.jp

Notes

The authors declare no competing financial interest.

■ ACKNOWLEDGMENTS

We thank K. Shibata and K. M. Cha for fruitful discussions and Y. Arakawa for his continuous encouragement. We are also grateful to S. Ishida for his experimental support and to K. Sato for being permitted to use the graphics of a C_{60} molecule. The numerical calculations were performed at Supercomputer Center, Institute for Solid State Physics, The University Tokyo, and at Information Technology Center, University of Tokyo. This work was partly supported by CREST program, JST, the Grants-in-Aid for JSPS Fellows, Project for Developing Innovation Systems of MEXT, and the Grants-in-Aid for Scientific Research on the Innovative Area "Materials Design through Computics: Complex Correlation and Non-Equili-

brium Dynamics" from MEXT (No. 23104501). Advanced Institute for Materials Research was established by World Premier International Research Initiative (WPI), MEXT.

REFERENCES

(1) Gimzewski, J.; Stoll, E.; Schlittler, R. *Surf. Sci.* **1987**, *181*, 267−277.
(2) Reed, M.; Zhou, C.; Muller, C.; Burgin, T.; Tour, J. *Science* **1997**, *278*, 252−254.
(3) Zhou, C.; Muller, C.; Deshpande, M.; Sleight, J.; Reed, M. *Appl. Phys. Lett.* **1995**, *67*, 1160−1162.
(4) Park, H.; Lim, A.; Alivisatos, A.; Park, J.; McEuen, P. *Appl. Phys. Lett.* **1999**, *75*, 301−303.
(5) Kubatkin, S.; Danilov, A.; Hjort, M.; Cornil, J.; Bredas, J.; Stuhr-Hansen, N.; Hedegard, P.; Bjornholm, T. *Nature* **2003**, *425*, 698−701.
(6) Park, H.; Park, J.; Lim, A.; Anderson, E.; Alivisatos, A.; McEuen, P. *Nature* **2000**, *407*, 57−60.
(7) Liang, W.; Shores, M.; Bockrath, M.; Long, J.; Park, H. *Nature* **2002**, *417*, 725−729.
(8) Heersche, H.; de Groot, Z.; Folk, J.; van der Zant, H.; Romeike, C.; Wegewijs, M.; Zobbi, L.; Barreca, D.; Tondello, E.; Cornia, A. *Phys. Rev. Lett.* **2006**, *96*, 206801.
(9) Grose, J.; Tam, E.; Timm, C.; Scheloske, M.; Ulgut, B.; Parks, J.; Abruna, H.; Harneit, W.; Ralph, D. *Nat. Mater.* **2008**, *7* (11), 884−889.
(10) Dediu, V.; Murgia, M.; Matacotta, F.; Taliani, C.; Barbanera, S. *Solid State Commun.* **2002**, *122*, 181−184.
(11) Xiong, Z.; Wu, D.; Vardeny, Z.; Shi, J. *Nature* **2004**, *427*, 821−824.
(12) Pasupathy, A.; Bialczak, R.; Martinek, J.; Grose, J.; Donev, L.; McEuen, P.; Ralph, D. *Science* **2004**, *306*, 86−89.
(13) Yamada, R.; Noguchi, M.; Tada, H. *Appl. Phys. Lett.* **2011**, *98*, 053110.
(14) Schmaus, S.; Bagrets, A.; Nahas, Y.; Yamada, T.; Bork, A.; Bowen, M.; Beaurepaire, E.; Evers, F.; Wulfhekel, W. *Nat. Nanotechnol.* **2011**, *6* (3), 185−189.
(15) Ono, K.; Shimada, H.; Kobayashi, S.; Ootuka, Y. *J. Phys. Soc. Jpn.* **1996**, *65*, 3449−3451.
(16) Barnas, J.; Fert, A. *Eur. Lett.* **1998**, *44*, 85−90.
(17) Yakushiji, K.; Ernult, F.; Imamura, H.; Yamane, K.; Mitani, S.; Takanashi, K.; Takahashi, S.; Maekawa, S.; Fujimori, H. *Nat. Mater.* **2005**, *4*, 57−61.
(18) Bernand-Mantel, A.; Seneor, P.; Bouzehouane, K.; Fusil, S.; Deranlot, C.; Petroff, F.; Fert, A. *Nat. Phys.* **2009**, *5*, 920−924.
(19) Wunderlich, J.; Jungwirth, T.; Kaestner, B.; Irvine, A.; Shick, A.; Stone, N.; Wang, K.; Rana, U.; Giddings, A.; Foxon, C.; Campion, R.; Williams, D.; Gallagher, B. *Phys. Rev. Lett.* **2006**, *97*, 077201.
(20) Sahoo, S.; Kontos, T.; Furer, J.; Hoffmann, C.; Graber, M.; Cottet, A.; Schonenberger, C. *Nat. Phys.* **2005**, *1*, 99−102.
(21) Strachan, D.; Smith, D.; Johnston, D.; Park, T.; Therien, M.; Bonnell, D.; Johnson, A. *Appl. Phys. Lett.* **2005**, *86*, 043109.
(22) Keane, Z. K; Yu, L. H.; Natelson, D. *Appl. Phys. Lett.* **2006**, *88*, 062514.
(23) Yoshida, K.; Umeno, A.; Sakata, S.; Hirakawa, K. *Jpn. J. Appl. Phys.* **2009**, *48*, 120216.
(24) Yoshida, K.; Umeno, A.; Sakata, S.; Hirakawa, K. *Appl. Phys. Express* **2010**, *3*, 045001.
(25) Umeno, A.; Hirakawa, K. *Appl. Phys. Lett.* **2009**, *94*, 162103.
(26) Heid, R.; Pintschovius, L.; Godard, J. *Phys. Rev. B* **1997**, *56* (10), 5925−5936.
(27) Roch, N.; Florens, S.; Bouchiat, V.; Wernsdorfer, W.; Balestro, F. *Nature* **2008**, *453* (7195), 633−U3.
(28) Yu, L. H.; Keane, Z. K.; Ciszek, J.; Cheng, L.; Stewart, M.; Tour, J.; Natelson, D. *Phys. Rev. Lett.* **2004**, *93*, 266802.
(29) Henkelman, G.; Arnaldsson, A.; Jonsson, H. *Comput. Mater. Sci.* **2006**, *36*, 254−360.
(30) Hunt, M.; Modesti, S.; Rudolf, P.; Palmer, R. *Phys. Rev. B* **1995**, *51* (15), 10039−10047.
(31) Julliere, M. *Phys. Lett.* **1975**, *54* (3), 225−226.
(32) Moodera, J.; Mathon, G. *J. Magn. Magn. Mater.* **1999**, *200* (1−3), 248 and references therein.
(33) Bolotin, K. I.; Kuemmeth, F.; Pasupathy, A. N.; Ralph, D. *Nano Lett.* **2006**, *6* (1), 123−127.
(34) Note that in SET devices even a slight shift in electrochemical potential can lead to a large resistance change around the bias conditions where $\partial I/\partial V_{SD}$ has peaks. In Figure 3, we can see enhanced TMR along the edge lines of the Coulomb diamond and a line in the transport regime indicated by a white arrow. This is likely to be due to the electrochemical potential shifts.
(35) Atodiresei, N.; Brede, J.; Lazic, P.; Caciuc, V.; Hoffmann, G.; Wiesendanger, R.; Blugel, S. *Phys. Rev. Lett.* **2010**, *105*, 066601.
(36) Kawahara, S. L.; Lagoute, J.; Repain, V.; Chacon, C.; Girad, Y.; Rousset, S.; Smogunov, A.; Barreteau, C. *Nano Lett.* **2012**, *12*, 4558−4563.
(37) Vanderbilt, D. *Phys. Rev B* **1990**, *41*, 7892−7895.
(38) Morikawa, Y.; Ishii, H.; Seki, K. *Phys. Rev. B* **2004**, *69*, 041403(R)−041406(R).
(39) Perdew, J. P.; Burke, K.; Ernzerhof, M. *Phys. Rev. Lett.* **1996**, *77*, 3865−3868.
(40) Grimme, S. *J. Comput. Chem.* **2006**, *27*, 1787−1799.
(41) Lee, K.; Murray, E. D.; Kong, L.; Lundqvist, B. I.; Langreth, D. C. *Phys. Rev. B* **2010**, *82*, 081101(R).
(42) Cooper, V. R. *Phys. Rev. B* **2010**, *81*, 161104(R).
(43) Hamada, I.; Otani, M. *Phys. Rev. B* **2010**, *82*, 153412.
(44) Hamada, I.; Otani, M.; Sugino, O.; Morikawa, Y. *Phys. Rev. B* **2009**, *80*, 165411.
(45) Otani, M.; Sugino, O. *Phys. Rev. B* **2006**, *73*, 115407.

dx.doi.org/10.1021/nl303871x | *Nano Lett.* XXXX, XXX, XXX−XXX